



HAL
open science

A novel low-cost material for thiophene and toluene removal: Study of the tire pyrolysis volatiles

Hiba Aouled Mhemed, Sana Kordoghli, Mylène Marin Gallego, Loubna Hadhoum, Jean François Largeau, Fethi Zagrouba, Mohand Tazerout

► To cite this version:

Hiba Aouled Mhemed, Sana Kordoghli, Mylène Marin Gallego, Loubna Hadhoum, Jean François Largeau, et al.. A novel low-cost material for thiophene and toluene removal: Study of the tire pyrolysis volatiles. Chemical Engineering Journal, 2022, 450, pp.138059. 10.1016/j.cej.2022.138059 . hal-04188294

HAL Id: hal-04188294

<https://hal.science/hal-04188294>

Submitted on 13 Oct 2023

HAL is a multi-disciplinary open access archive for the deposit and dissemination of scientific research documents, whether they are published or not. The documents may come from teaching and research institutions in France or abroad, or from public or private research centers.

L'archive ouverte pluridisciplinaire **HAL**, est destinée au dépôt et à la diffusion de documents scientifiques de niveau recherche, publiés ou non, émanant des établissements d'enseignement et de recherche français ou étrangers, des laboratoires publics ou privés.

A novel low-cost material for thiophene and toluene removal : study of the tire pyrolysis volatiles

Hiba AOULED MHEMED ^{1, 2, 3, *}, Sana KORDOGHLI ^{3, 4}, Mylène MARIN GALLEGO ⁵,
Loubna HADHOUM ¹, Jean François LARGEAU ^{1, 6}, Fethi ZAGROUBA ³, Mohand
TAZEROUT ¹

¹ GEPEA-CNRS UMR 6144, IMT Atlantique, Nantes, 44300, France.

² National School of Engineers of Gabes, University of Gabes, 6026 Gabes, Tunisia

³ Research Laboratory for Sciences and Technologies of Environment LR16ES09, High Institute of Sciences and Technologies of Environment, Carthage University, Borj Cedria, Tunisia.

⁴ National School of Sciences and Advanced Technologies, Borj Cedria, University of Carthage, Tunisia.

⁵ Chemical Engineering Laboratory, University of Toulouse, CNRS, INPT, UPS, Toulouse, France

⁶ Icam, 35 rue du Champ de Manœuvres, 44470 Carquefou, France.

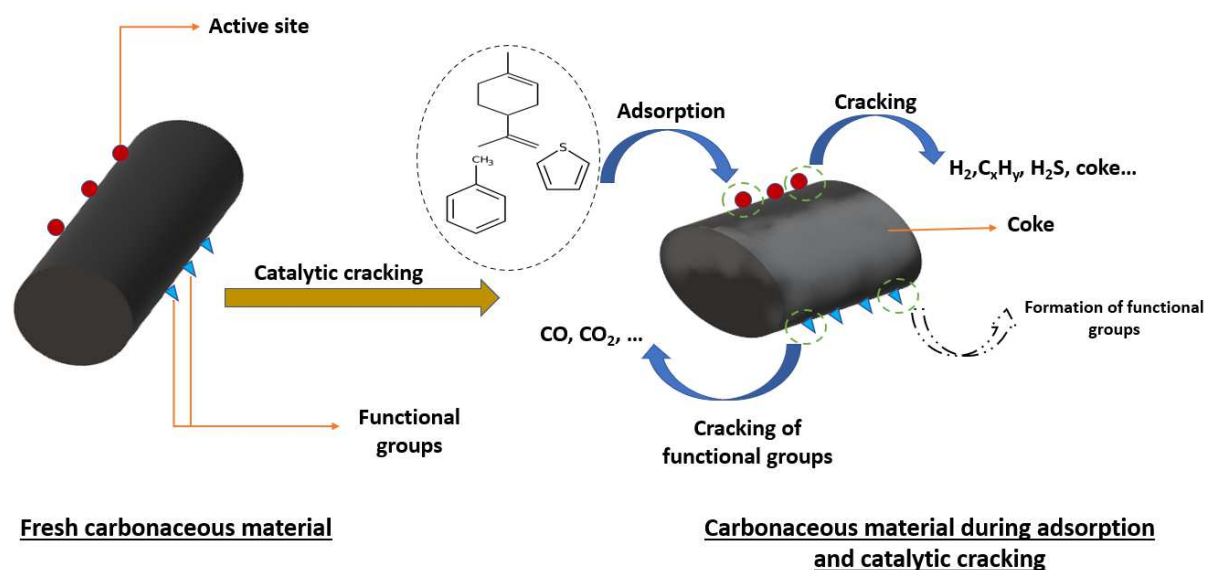
* *Corresponding author* : Hiba AOULED MHEMED, aouled_mhemed.hiba@hotmail.com

Abstract

It remains challenging to produce new and efficient adsorbents to remove sulfur compounds from waste tire pyrolysis oils. The present work investigated the ex-situ treatment by desulfurization and cracking of volatiles from the pyrolysis of waste tires using an innovative synthetic oil mixture. For this purpose, biochars from the pyrolysis of abundant biomasses (date seeds and spent coffee grounds) were used to improve the quality of these volatiles. Furthermore, the purification efficiency of these biochars was compared to that of commercial activated carbon. Thus, the influence of the operating conditions was studied. Finally, to

provide an innovative insight into the desulfurization efficiency, the regeneration of the best performing desulfurization material was carried out. The results show promising desulfurization and cracking capacities of the spent coffee grounds biochar and excellent regeneration performance.

Graphical abstract



Abbreviations :

UT, Used Tires; UTPO, Used Tires Pyrolysis Oil; CG, Spent Coffee grounds; BC_CG, Biochar derived from spent coffee grounds; DS, Date Seeds, BC_DS, Biochar derived from date seeds; AC, Commercial Activated Carbon; TDV, Volatiles Derived from the pyrolysis of used Tires.

Keywords : waste tires, desulfurization, biochar, cracking, regeneration

1. Introduction

Nowadays, energy and environment are key consideration in discussions of sustainable development. An inevitable increase in used tires is a severe environmental problem. Around 1.5 billion tires are produced worldwide each year, which corresponds to approximately 17 million tons of used tires (UT). In 2013, used tires in European Union countries reached 3.6 million tons [1]. The main routes for waste tires management are landfilling, energy recovery,

material recovery, retreading, and reuse/export. Meanwhile, the composition of tires makes their energy recovery a profitable business. To minimize the negative impacts of this waste on the environment, pyrolysis can be considered the most promising practice.

Among the products formed through scrap tire pyrolysis, pyrolysis oil has been considered a promising alternative fuel since its fuel characteristics are similar to commercial diesel. Its composition consists of paraffin, alkenes, and aromatic compounds. Its high calorific value of around 41-44 MJ/kg attracts its use as a substitute for conventional liquid fuels [2]. However, despite its high energetic value, sulfur, nitrogen, and heavy hydrocarbons make this oil unsuitable for use as vehicles fuel [3]. Indeed, sulfur comes from the rubber vulcanization step in tire manufacturing: rubber monomers are crosslinked with sulfur during the vulcanization process to obtain mechanical strength and improve the thermostatic properties of rubber [4]. Some authors have reported the sulfur content in used tires pyrolysis oil (UTPO) to be 0.3 wt% [5], but the majority of reported values are around 1.4 wt% [6]. Sulfur is usually converted to H_2S , CH_3SH , COS , and SO_2 during pyrolysis [7]. Sulfides (CS_2 , H_2S) and thiophene are the main sulfur species in solid pyrolytic residues, while thiophene and sulfites (SO_2) are the predominant sulfur compounds in the UTPO [8]. Hence, the choice of thiophene as the main sulfur compound of the UTPO can also serve as a model for other sulfur species such as CS_2 , COS , or mercaptans.

According to several studies, UTPO can be desulfurized using the conventional sulfur removal methods for petroleum fuels. Currently, the industrial process (Technology Readiness Level (TRL) 9) commonly used for the removal of sulfur from petroleum fractions is hydrodesulfurization (HDS). This catalytic process has been used in refineries since 1993 to remove sulfur compounds such as sulfides and disulfides from petroleum fractions. The temperature and hydrogen pressure of HDS are usually kept in the range of 300 to 400 °C and 5 to 13 MPa, respectively. The hydrodesulfurization catalysts are usually Co or Ni promoted

Mo or W sulfide. γ -Al₂O₃ is the traditional support material for HDS catalysts as it provides a high surface area and high thermal and mechanical stabilities [9]. Although refineries around the world commercially apply the HDS process, its requirements make it a costly operation. In this regard, several desulfurization techniques have been developed. All methods other than HDS are still in the technological development phase (TRL4 and TRL5) [10]. The adsorption process has become a promising approach to ultra-deep desulfurization in this context. This economical method, environmentally friendly, can reduce the sulfur content to <1 ppm [11]. Desulfurization by adsorption, however, faces two significant challenges :

1. develop high-capacity adsorbents ;
2. identify adsorbents that are more selective towards the adsorption of sulfur compounds (mainly aromatics) in a fuel containing several other aromatic and olefinic compounds.

Hence, there is a constant effort to invent new adsorbents to remove thiophenes from fuels [12]. The most widely used adsorbents in the industry are activated carbons, zeolites, silica gels, activated alumina, and metal-organic frameworks (MOFs). Although their efficiency, these materials have relatively high manufacturing costs. Whence, the interest to develop an economical adsorbent with a high absorption and regeneration capacity. A novel approach to using biomass waste as a source of adsorbents for toxic gases and various liquids has been developed [13]. The term biochar has been used to refer to these increasingly popular and profitable materials. Biomass, abundantly available, is a promising source of biochar production. Among the most relevant substitution opportunities in Tunisia, the biomass generated annually by Tunisian phoenix culture and coffee grounds are renewable energy sources that can represent both environmental and economic benefits [14]. Currently, Tunisia ensured the production of around 250 000 tons of dates in 2016 [15]. This significant production generates substantial solid waste, such as date seeds and branches, discarded or mixed with animal feed. On the other hand, coffee is the second most-consumed product

worldwide. Therefore, a considerable amount of this residue is generated. The annual worldwide generation of spent coffee grounds through soluble coffee production industries is approximately 6 million tons which can pose several problems in terms of proper disposal [16].

Given the complexity and non-reproducibility of pyrolytic oils, a synthetic liquid representative of tire pyrolysis oils and sulfur pollutants is essential for understanding potential competition during desulfurization. Our findings presented in this study are very different from those described in the literature until now. In this paper, it is highlighted that there is no study concerning the use of biochar as an adsorbent for the hot dynamic adsorptive desulfurization of the volatile fraction resulting from the tires pyrolysis, which has been reported in the literature. This study was performed to obtain helpful information for designing industrial carbon-based sulfur and tar removal system. Moreover, it exposes novelty because it developed a promising eco-friendly alternative fuel from waste tires using high-efficiency and low-cost adsorbents. These materials were tested in a synthetic liquid representative of tire pyrolysis oils. A commercial activated carbon was used as an adsorbent for comparison. The adsorption and cracking experiments were performed under an inert atmosphere. The data obtained were used to compare the performance of the different carbonaceous materials and to understand the relationship between their properties and their effectiveness in reducing sulfur and tars. The results provided valuable information on the deactivation mechanism and the interaction between aromatics and the surface of the biochar. The regeneration of the best sulfur adsorbent by two methods was also evaluated.

2. Materials and Methods

2.1 Biochars and activated carbon

Two carbonaceous materials were tested in the setup. The feedstock for the production of biochars are wastes generated by Tunisian phoeniculture (date seeds) and by soluble coffee

production industries (spent coffee grounds). The powder of spent coffee grounds was pelletized before the production of biochar. The obtained pellets have a diameter of 4 mm and a length between 5 and 10 mm.

The production of biochar was carried out by pyrolysis at 750 °C, and a heating rate of 5 °C/min, for 3 hours. This temperature is chosen to ensure that no additional pyrolysis reactions take place during the desulfurization tests. Fig. S1 represents the biochar production reactor. Pyrolysis-derived biochar will be referred as BC_GC (biochar derived from spent coffee grounds) and BC_DS (biochar derived from date seeds). The extruded commercial activated carbon (AC) has been provided by EHEIM AKTIV. The particle diameter of the carbonaceous materials is between 2 and 3 mm.

2.2 Adsorbents characterizations

Biochars and commercial activated carbon are complex materials whose physicochemical properties may be involved in the purifying mechanisms by adsorption. Therefore, a multi-scale characterization was carried out (Fig. S2). The different carbonaceous materials were characterized in terms of composition and surface properties. The description of the elementary analysis, immediate analysis, potential hydrogen (pH), and the point of zero charge (pHpzc) have been developed in previous work [17,18]. Before elementary and mineral analysis, biochars were reduced to powder in a ball mill model Retsch MM400. Minerals were determined using X-ray fluorescence spectrometry model EDX-800HS2 (Shimadzu, USA). The characterization of textural properties was determined by the Brunauer, Emmett and Teller theory (BET) theory using the Micromeritics Smart VacPrep instrument. Morphological characterization of solid samples was performed using the scanning electron microscopy (SEM) technique (JEOL JSM 5800LV). Oxygen groups on the surface of biochars and AC were evaluated using the Boehm-titration method [18].

2.3 Experimental setup

Fig.1 shows the process diagram of synthetic pyrolytic liquid treatment by desulfurization and cracking. The experiments were carried out in a vertical fixed bed reactor. The dimensions of the bed are an internal diameter of 3.8 cm and a maximum height of 30 cm. The diameter of the carbonaceous material particle is approximately between 2 and 3 mm. The catalytic bed is perforated to ensure a good gas distribution and avoid preferential paths. Three thermocouples were used to measure the temperature at the core, the bottom, and the head of the catalytic bed (TE2, TE3, and TE1, respectively). In addition, two pressure sensors are placed upstream and downstream of the reactor to calculate the pressure drops (ΔP) induced by the system and to detect any pressure drops during the tests. The nitrogen is continuously preheated to 200 °C before entering the reactor. The heating operation lasts 90 min until temperature stabilization (500 °C). The synthetic mixture was injected into the gas stream using a syringe pump when the system was stable. The ascending gas is purified by crossing the fixed bed. An electrical box exempts the control and regulation of the gas preheater and the heating of the cracker. The acquisition interface permits the monitoring and recording of the internal (TE1, TE2, TE3, TE4), upstream, and downstream temperatures (TE5, TE6) of the reactor, as well as the differential pressure between the inlet and the outlet of the reactor (ΔP). At the exit of the reactor, the gaseous effluent is analyzed online by a micro-GC (R-3000, SRA Instruments). The reactor operating pressure is the atmospheric pressure. For safety reasons, ventilation is kept active throughout the experiments.

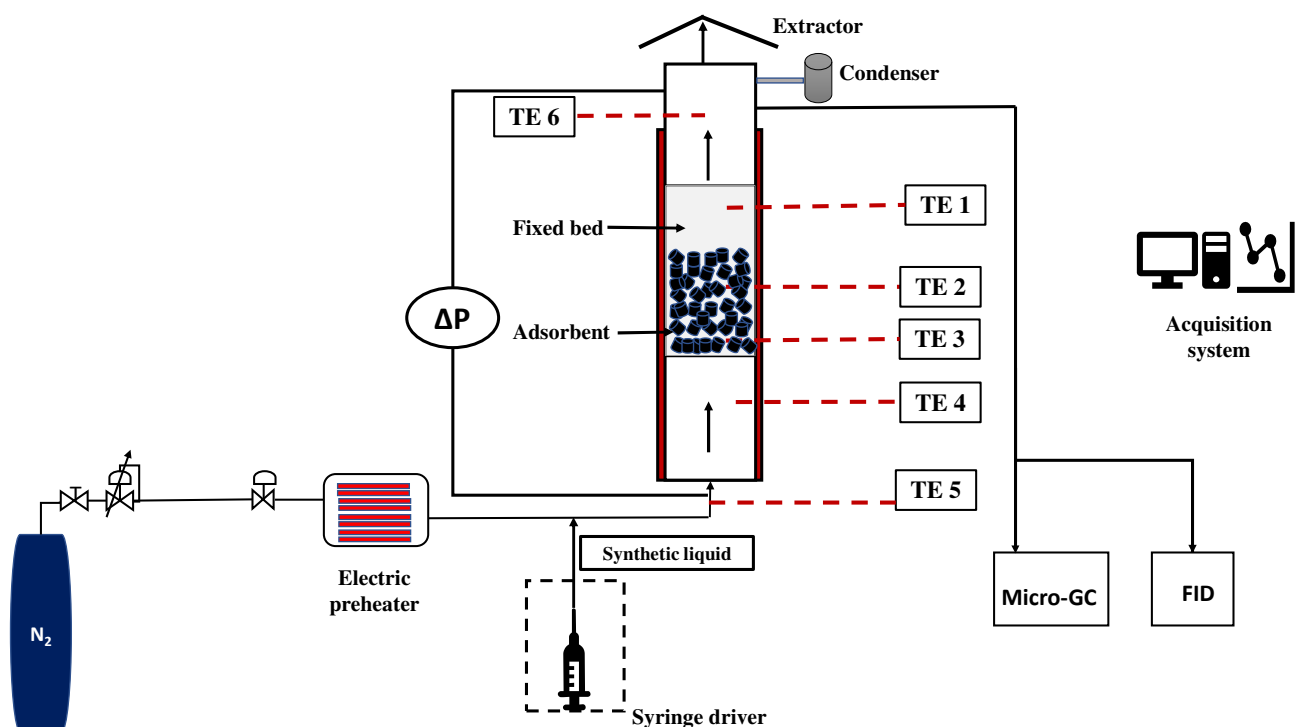


Fig. 1. Representative diagram of the post-pyrolysis reactor.

Two synthetic feed solutions were prepared as follows :

- Mixture 1 : Thiophene + Toluene
- Mixture 2 : Thiophene + 40 % Toluene + 60 % Limonene

The N_2 flow was continued for all the test. The concentration of the injected toluene was set at $9800 \pm 1\%$ ppm in mixture 1. However, the concentrations of toluene and limonene in mixture 2 were calculated to be $3940 \pm 1.20\%$ ppm and $5860 \pm 1.35\%$ ppm, respectively. The thiophene adsorption capacities of the different adsorbents were determined for an initially fixed concentration of $500 \pm 0.5\%$ ppm [19–21]. The bed height ($h= 20$ cm), the reactor temperature ($T=500$ °C), and the duration of the experiment (60 min) are kept unchanged during the various tests.

Table 1 summarizes the operating conditions.

Table 1. Overview of experimental conditions.

Materials	BC_CG	BC_DS	AC
Operations conditions			
h (cm)	20.00 ± 0.20	20.00 ± 0.20	20.00 ± 0.20
m (g)	56.00 ± 0.13	95.00 ± 0.17	105.20 ± 0.12
Flow rate (Q _v) (Nm ³ /h)	0.20 ± 0.005	0.20 ± 0.005	0.20 ± 0.005
	0.10 ± 0.001	0.10 ± 0.001	0.10 ± 0.001
Residence time (t _s) (s)	1.25 ± 0.02	1.25 ± 0.02	1.25 ± 0.02
	2.50 ± 0.07	2.50 ± 0.07	2.50 ± 0.07
Synthetic mixture			
Mixture 1	X	X	X
Mixture 2	X	X	X

2.4 Adsorption and cracking experiments

The breakthrough curves obtained from the micro-GC measurements were used to calculate the total adsorption capacity W_s (mg/g_{adsorbent}) which is defined by [22] :

$$W_s = \frac{U_0 \times C_0 \times \int_0^{t_e} \left(1 - \frac{C(t)}{C_0}\right) dt}{h \times \rho} \quad (1)$$

The adsorption capacity at the breakthrough point (mg/g) is :

$$W_p = \frac{U_0 \times C_0 \times \int_0^{t_p} \left(1 - \frac{C(t)}{C_0}\right) dt}{h \times \rho} \quad (2)$$

Where C_0 and $C(t)$ are the concentration of thiophene at the inlet and outlet of the reactor, respectively (g/cm³), U_0 is the inlet flow velocity (cm/s), h is the bed height (cm), ρ is the density of the adsorbent (g/cm³), t_p is the break point–time (min) where effluent concentration

was about 5 % of the influent concentration while t_e (min) is the exhaustion time where the effluent concentration equals about 95 % of the influent concentration. The integration of the vacuum breakthrough curve was also performed to take into account the residence time of the gas flow in the whole vacuum system. The blank test residence time in the entire installation (pipes, reactor, and preheater) was deduced from the obtained breakthrough curves. Integration was carried out by performing the trapezoid method on each breakthrough curve. In industrial practice, a bed is operated until an effluent reaches an arbitrarily chosen low concentration value known as the breakpoint concentration. It is the maximum allowable concentration that the effluent can reach. At this breakpoint, the bed is not fully used for effluent uptake. Then, the term called Length of Unused Bed (LUB) is then calculated by the following equation:

$$LUB = h \times \left(1 - \frac{W_p}{W_s} \right) \quad (3)$$

The adsorption efficiency is given by the relationship below [23] :

$$\eta_{adsorption} (\%) = 100 \times \frac{W_s \times m}{C_0 \times Q_v \times t_e} \quad (4)$$

Where Q_v is the total volumetric inlet flow rate (cm^3/h), m is the mass of adsorbent in the fixed bed (g).

Once the best thiophene adsorption operating conditions were identified, a gas chromatograph (GC, Perkin Elmer Clarus 680) coupled with a mass spectrometer (MS, Perkin Elmer Clarus 600 S) equipped with an FID was used to identify the cracking products detected by the micro-GC but not identified or quantified. Thus, gas samples were taken at the outlet of the reactor. The sample composition was processed in an SBLTM-5ms Capillary Column, 30 m long, 0.25 mm internal diameter, and 0.25 μm film thickness. The temperature of the GC-MS oven was maintained at 50 °C for 2 min. Then, the temperature was raised to 110 °C at 2 °C/min, followed by 100 °C/min to 280 °C, maintained for 10 min. The injector temperature

is 200 °C. The split mode is splitless. On each test, 10 µl of the gas sample was injected. For the column, the flow rate of carrier gas (helium) was 1.0 ml/min [24].

2.5 Adsorbent regeneration

A preliminary laboratory study allowed us to fix regeneration's most critical operating conditions. Indeed, the regeneration of the best adsorbent was studied at the predefined desorption temperature (720 °C) in two gas atmospheres :

- a. 15 vol.% CO₂ in N₂ ;
- b. Pure N₂.

To ensure a non-brutal regeneration, a constant gas volume (0.08 ± 0.003 Nm³/h) was introduced in the reactor. Thus the regeneration cycle was carried out with various adsorption and desorption cycles according to the steps presented in Fig. S3.

3. Results and discussions

3.1 Sorbents characterization

The composition of the biochars and the commercial activated carbon are presented in Table 2. The BC_DS contains one of the highest amounts of carbon and one of the lowest ashes among the samples, while BC_GC contains the lowest amount of carbon and the highest of ashes. Ash is the inorganic part of biomass left as a solid residue after the thermal conversion. Ash is primarily made of silica, aluminum, iron, and calcium compounds, but small amounts of magnesium, titanium, sodium, and potassium may be present [25]. Since the structure of ash compounds is crystalline, a significant presence of crystalline phases is expected in samples rich in ash, such as BC_GC. To confirm these findings and obtain further information on the possible crystalline phases present in the samples, XRD analysis is recommended in future work. The aromaticity and polarity of the adsorbents were evaluated by calculating the H/C and (O + N)/C molar ratios, respectively. The molar ratios of H/C for BC_CG, BC_DS and AC are 0.02, 0.02 and 0.01, respectively. Efficient carbon sorbents are characterized by

strong carbonization and high aromaticity if the molar ratio of H/C is less than 0.5 [26]. The polarity index $[(O + N)/C]$ for BC_CG, BC_DS and AC were 0.10, 0.08 and 0.12, respectively. The higher polarity index for BC_CG, and AC compared to that for BC_DS implies that BC_CG, and AC are more hydrophilic and contain more polar functional groups for coordination with thiophene, which should be confirmed by Bohem-titration results. Overall, the pH of all biochars is around 7. A decrease in acidity (biomass with a pH around 5) after pyrolysis (biochar with a pH ranging from 7 to 7.5) is noted.

Table 2. Elemental analyzes, pH, and humidity of biochars and commercial activated carbon.

Materials	CG	BC_CG	DS	BC_DS	AC
Elemental and proximate analysis					
C	50.40±0.28	82.72±0.50	47.92±0.53	87.27±0.38	85.53±0.14
H	6.90±0.15	1.61±0.03	6.60±0.22	1.51±0.01	0.70±0.00
N	2.40±0.05	2.79±0.07	0.90±0.00	1.62±0.01	0.27±0.00
S	nd ²	nd	nd	nd	nd
O ¹	38.48±0.67	5.88±0.12	43.38±0.27	5.60±0.02	9.90±0.06
ash	1.80±0.03	7.00±0.24	1.20±0.02	4.00±0.06	3.60±0.02
H/C	0.14	0.02	0.14	0.02	0.01
(O+N)/C	0.81	0.10	0.92	0.08	0.12
pH	5.12±0.16	7.45±0.15	4.32±0.06	7.40±0.21	7.15±0.11
pH _{pzc}	nm ³	7.50±0.23	nm	7.40±0.27	7.00±0.13
Textural analysis					
S _{BET} (m ² /g)	nm	49.44±0.22	nm	225.63±3.14	816.67±2.50
V _{total} (cm ³ /g)	nm	0.038±0.00	nm	0.14±0.00	0.46±0.00
V _{micro} (cm ³ /g)	nm	0.004±0.00	nm	0.07±0.00	0.20±0.00
V _{meso} (cm ³ /g)	nm	0.026±0.00	nm	0.06±0.00	0.14±0.00
Average pore diameter (nm)	nm	3.098±0.45	nm	2.56±0.027	2.27±0.035

¹ O (%) = 100 % - C (%) - H (%) - N (%) - S (%) - ash (%);

² nd : not detected; traces: concentration below 0.06 wt %;

³ nm : not measured;

V_{micro} by t-plot;

V_{meso} by BJH.

The analysis of the ash composition using X-ray fluorescence spectrometry is represented in Fig. S4. The potassium (K) is the main element in BC_CG and BC_DS (3.12 and 2.57 wt%, respectively), while AC is mainly rich in iron (4.73 wt%). The amount of sulfur and calcium

in AC is not negligible. Minerals such as Ca, Mg, and K can improve the catalytic activities of carbonaceous materials [27]. Transition metals (Fe, Al, Co, Ni, Zn) are essential for catalytic cracking reactions. Some of these species are present in AC with appreciable quantities (4.73 wt % of Fe) and lower amounts in biochars. Thus, AC is theoretically a good candidate for tar cracking. Nitrogen adsorption indicates that the microporous volume of AC is significantly higher than other materials used in this study (Table 2). The BC_CG has the lowest specific surface area (49.44 m²/g). Its microporous volume is about fifty times smaller than that of AC. Its mesoporous volume is about five times smaller than commercial activated carbon. The average pore diameters of the three materials are more significant than 2 nm. So these adsorbents have more pores in the mesoporous region.

Fig. S5 illustrates the slow nitrogen diffusion inside the pores. Also, a sharp increase in the amount of nitrogen adsorbed near saturation was observed. This may be associated with the condensation in the inter-particle voids [28]. The hysteresis phenomenon is generally associated with the capillary condensation in mesoporous structures [29]. Fig. S5 (a) shows that the BC_CG has the greatest hysteresis, followed by BC_DS (Fig. S5 (b)). The hysteresis loop of these two samples appears to belong to type-H4. This type of deformation is often attributed to narrow, slit-shaped pores and the presence of mesopores. Thus, imprisoned nitrogen cannot be released due to its affinity with the biochar heterogeneous surface properties [30]. Most probably, the pore wall of biochar traps nitrogen molecules. Moreover, the isotherms of BC_CG and BC_DS are type I (according to the IUPAC classification). This indicated a certain microporosity of these biochars, with a progressive saturation of the substantially equivalent adsorption sites. The nitrogen adsorption isotherm of AC (Fig. S5 (c)) is also type I: it has a slightly horizontal plateau, indicating the presence of very narrow micropores [31].

Density Functional Theory (DFT) has also been applied to N₂ adsorption data. The DFT model is based on the thermodynamics equation, which calculates the amount of specific adsorption in a range of pores by solving the distribution function of gas density in a particular pore space [32]. Fig. 2 illustrates the pore size distributions obtained by DFT. All three materials have a distribution towards pore sizes greater than 2 nm, with a more marked distribution for AC. The size distribution of pores confirms that they are predominantly mesoporous for the three materials. The AC has much narrower and smaller ultra-micropores (~0.6 nm). The BC_CG and BC_DS reveal a relatively identical mesoporous volume (0.002-0.0035 cm³/g), while AC is more extensive (0.015 cm³/g). All samples have a micropore size range from 0.4 nm to 2 nm with multiple peaks and a predominant maximum of ≤1.27 nm. In addition, BC_DS presents a non-negligible distribution of the macropores. This change in the pore size distribution may be due to a structural deformation that transforms mesopores into macropores [33].

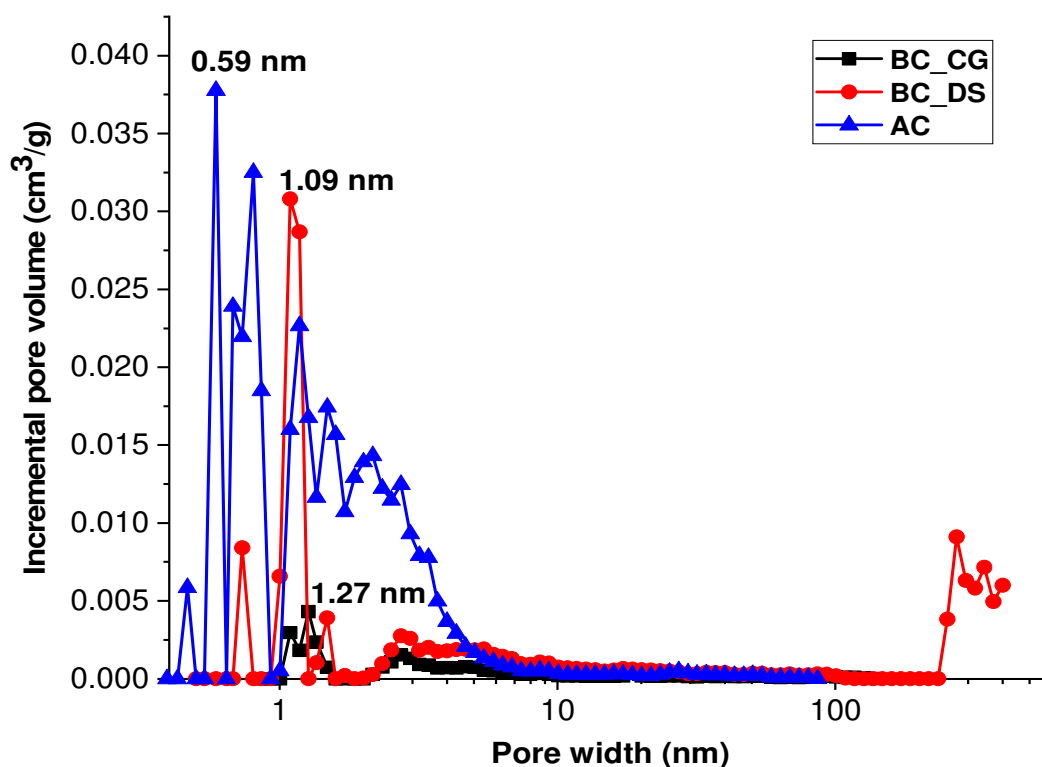


Fig. 2. Pore size distribution of BC_CG, BC_DS, and AC.

The surface topology of the tested materials and their macrostructure were described using SEM analysis (Fig. S6). The morphology of BC_CG indicates its heterogeneous surface and porous nature. It shows the development of a macro-porosity between 2 and 5 μm . On the other hand, the BC_DS has a structure with very few pores on the smooth surface. However, AC seems more homogeneous with a low macro-porosity.

The oxygenated groups present on the surface of carbonaceous materials are lactones, carboxylic or phenol acids, and basic groups such as carbonyl, quinone, and pyronic structures. They can affect the catalytic properties of adsorbents [34]. The characterization of the various used materials functional groups by Boehm titration is given in Table 3. Based on these results, BC_CG had the most significant amount of groups with a strong acidic character (carboxylic groups : 0.35 mmol/g). These functional groups can interact with the gaseous matrix and then increase the adsorption capacity and the conversion of the aromatic ratio [27]. On the other hand, the different materials (BC_DS and AC) are richer in compounds with a weak acid character, such as phenolic and lactonic groups (case of BC_DS). Though AC had high O content to the biochars (Table 2), much fewer oxygen, functional groups were observed in AC than in BC_CG. It may probably be because oxygen in AC exists in quinines or alcoholic hydroxyl, which could not be obtained by Boehm titration.

Table 3. Results of Boehm titration of various materials.

Adsorbents	BC_CG	BC_DS	AC
Surface acidity (mmol/g)	0.37±0.04	0.10±0.01	0.21±0.07
Surface basicity (mmol/g)	0.16±0.06	0.33±0.07	0.48±0.02
Carboxylic groups (mmol/g)	0.35±0.09	0.14±0.03	0.20±0.04
Lactone group (mmol/g)	0.23±0.05	0.15±0.07	0.00±0.00
Phenolic group (mmol/g)	0.12±0.03	0.22±0.08	0.42±0.06

3.2 Effect of the mixture composition on thiophene removal efficiency

The breakthrough curves of BC_CG, BC_DS, and AC obtained with the different gas matrix are shown in Fig. 3. The matrix composition had no notable impact on the removal capacity of BC_DS, which was almost stable at $0.80\text{--}0.83 \pm 0.01$ mg thiophene.g⁻¹. Compared to mixture 1, the efficiency of BC_CG was practically improved in the second mixture (1.38 versus 0.97 ± 0.02 mg thiophene.g⁻¹, respectively). Thus, at the break point, 49 % of the bed capacity is used which approximately corresponds to an unused section of length (LUB) of 9.80 cm. Within experimental error, for such a front, LUB can be used to design the full-scale adsorber from the breakthrough curves obtained in small-scale laboratory experiments by adding LUB to the length of bed needed to achieve the required capacity.

This improvement may be due to the complexity of the second matrix and, subsequently, the growth of the competitive adsorption between toluene and limonene, whose critical adsorption diameters are 0.67 nm and 0.68 nm, respectively [35]. Conversely, this competition becomes less pronounced for thiophene, whose required diameter is 0.53 nm. The breakthrough time of the AC was longer, indicating better retention of thiophene compared with biochar in the second matrix. The decline in biochar's breakthrough times reduces their adsorption capacities at the breakthrough point and consequently increase in the unused bed length. The AC's adsorption capacity has dramatically improved from a less complex mixture to a more complex blend (1.06 versus 0.60 ± 0.01 mg thiophene.g⁻¹, respectively). Its developed morphology may explain this comportment. The adsorption of organic compounds onto natural adsorbents has been described as a complex process, mainly controlled by chemical interactions and physical factors. The properties of the adsorbate molecules and the adsorbent, such as surface chemistry, specific surface areas, and porosity, often play critical roles. Studies on the part of physical factors, especially molecular size, aromatic compounds' structure, and adsorbents' pore structure, are relatively limited. Thus, the competitive effect of

toluene and limonene with thiophene during adsorption was further investigated. Despite the variation in feed composition, BC_CG still has the best desulfurizing capacities. The large BC_CG surface acid groups may explain this result. Indeed, these groups contribute to a better selective adsorption of thiophene owing to the stronger acid-base interaction. Similar results were found by Shang et al.[36] comparing biochars with low specific surface area to activated carbon for H₂S elimination.

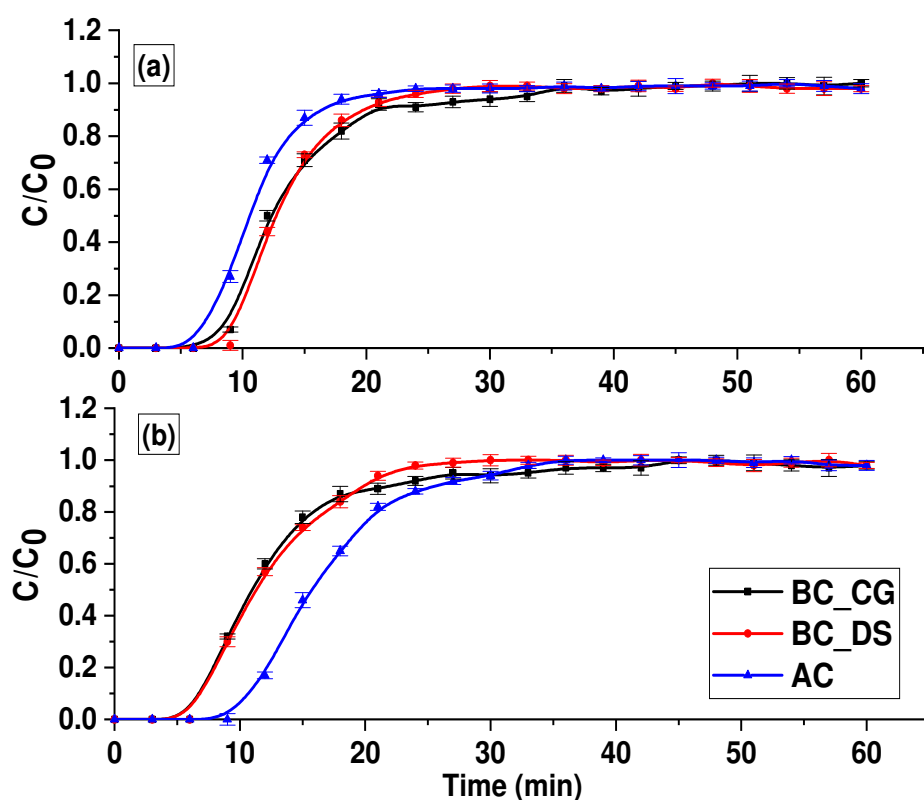


Fig. 3. Breakthrough curves of thiophene at 500 °C; 0.20 Nm³/h; (a) synthetic mixture 1; (b) synthetic mixture 2.

3.3. Effect of the residence time

Fig.4 shows the effect of residence time on the thiophene breakthrough curves in different synthetic mixtures. It is noted that the increase in residence time negatively influences the breakthrough time of BC_DS in both synthetic mixtures against an improvement in breakthrough time of BC_CG and AC. BC_DS has the lowest breakthrough time and therefore the smallest bed capacity used (38.60 %), which is equivalent to the most extended

LUB of 12.30 cm. Thus, the decrease in adsorption capacity can be explained by a predominance of the axial dispersion phenomenon over the mass transfer and consequently a reduction of the adsorbate diffusion in the adsorbent [37]. AC has the longest breakthrough time (approximately 19 min, mix 2). Therefore, it provides the best-utilized capacity of the bed (53%), suggesting better resistance to mass transfer [38]. However, no noticeable impact is perceived on the desulfurizing capacities of AC, which remained almost stable at $1.08\text{-}1.07 \pm 0.02$ mg thiophene.g⁻¹ (Fig. 4a and Fig. 4b). This is because as the flow rate decreases, the contact time in the catalyst bed is longer, and intraparticle diffusion becomes more efficient. Thus, the pollutant has more time to diffuse in the middle of the carbon particles, and hence a better adsorption capacity. Based on the amounts of thiophene adsorbed at breakthrough time and saturation, it is clear that increasing the residence time has a positive effect on the diffusion of thiophene and subsequently on its adsorption by the BC_CG. Indeed, this adsorbent shows the better thiophene removal by 1.44 ± 0.02 mg thiophene.g⁻¹ (see Fig. 4b) which corresponds to a desulfurization efficiency of 77.10 ± 0.5 % (mixture 2; $t_{s2} = 2.50$ s). Several authors have suggested that :

- (i) the adsorption of a solute on solid takes place in two steps which are the surface fixation and then the diffusion through the internal layers of the adsorbent;
- (ii) the limiting factor is the contact time between the two phases (gas and solid).

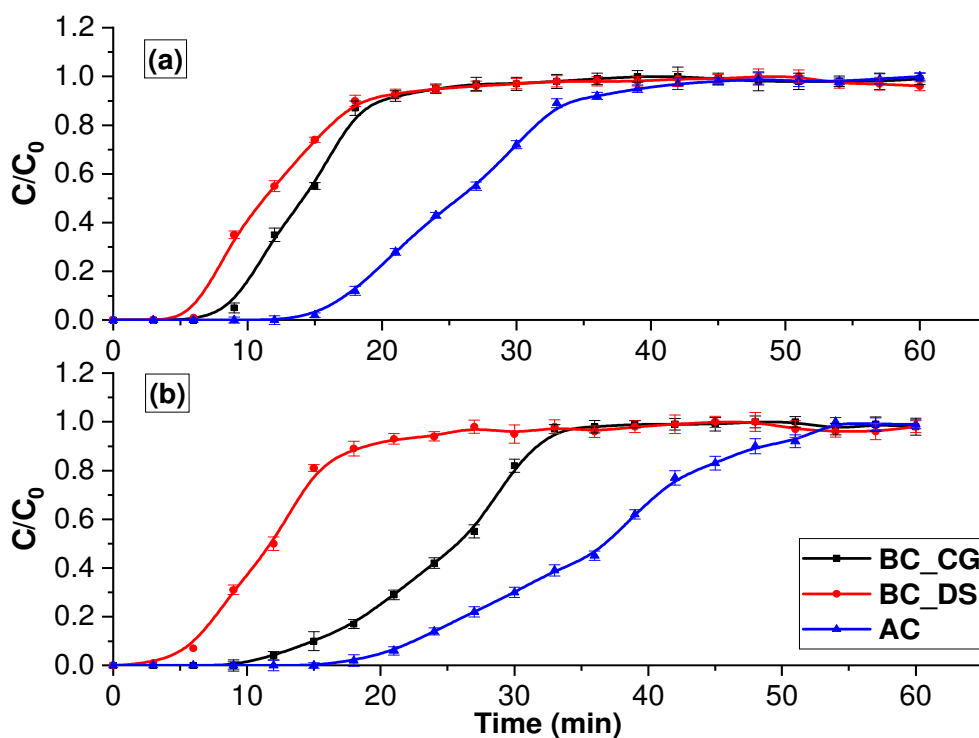


Fig. 4. Thiophene breakthrough curves at $T= 500\text{ }^{\circ}\text{C}$; $Q_v= 0.1\text{ Nm}^3/\text{h}$; (a) mixture 1; (b) mixture 2.

While thiophene adsorption has been studied for deep desulfurization in liquid phase for transport fuels [39,40], the literature on gas phase adsorption remains very scarce. A comparison of thiophene adsorption capacities with the literature is given in Table S1. Adsorption is by nature an exothermic reaction. However, despite the severe operating conditions used ($T= 500\text{ }^{\circ}\text{C}$), the adsorption capacities of thiophene by BC_CG are promising compared to other adsorbents reported in the literature.

3.4 Aromatic cracking

During experiments carried out under the best adsorption operating conditions ($Q_v = 0.1\text{ Nm}^3/\text{h}$; $t_s = 2.50\text{ s}$; $T= 500\text{ }^{\circ}\text{C}$; synthetic mixture 2), the concentration of both toluene and limonene at the outlet of the system evolved differently. It is worth pointing out that in mixture 1 no gases other than N_2 were detected with micro-GC in the exit gas. Only under these conditions, small amounts of H_2 and CO_2 were detected at the outlet of the system. H_2 concentration in the exit gas exhibited different trends over time with BC_CG, and AC,

peaking around 0.13 vol% during the beginning of the experiment for AC, to decrease gradually afterward and stabilizing around 0.03–0.04 vol%. However, hydrogen was stable for BC_CG (around 0.01 vol%) with no traces for BC_DS. The detection of H₂ as the main reaction product and the lack of light hydrocarbons in the exit gas confirm the mechanism of decomposition of aromatics over biochar with dehydrogenation and coke formation through condensation/polymerization reactions. The CO₂ is weakly produced (0.04 vol% for BC_CG; 0.01 vol% for BC_DS; and 0.07 vol% for AC). As a reminder, CO₂ is the product of catalytic cracking resulting from the reaction between the deposited coke and the oxygenated functions of the carbonaceous surface. In these conditions, the toluene and limonene conversion values for BC_CG and BC_DS remained lower than for AC indicating a mild activity of these biochars surfaces (see Fig. 5 (a, b)). It is also interesting to notice the trend of both BC_CG and AC with a toluene curve stabilizing at α above 5 % for more than an hour (see Fig. 5 a). These trends indicate that in these two materials, carbon deposition could support the decomposition of toluene. BC_DS exhibited a fast deactivation, as it converged with the toluene conversion value in about 37 min. For limonene, complete conversion was maintained for AC all along with the test. Both BC_CG and BC_DS sustained complete limonene conversion for a shorter time (about 35 and 15 min, respectively) (see Fig. 5 b). It appears as limonene was converted more efficiently than toluene. This observation agrees with the increased reactivity of chars towards compounds with increased aromaticity. GC-MS analysis of limonene cracking products indicates the production of a variety of compounds such as β -terpinene, γ -terpinene, α -phellandrene, camphene, and α -terpinolene. Hydrogen displacement can occur in α -terpinolene, leading to a displacement of hydrogen within the ring to obtain γ -terpinene as a second isomer. However, α -phellandrene can be formed from the isomerization of γ -terpinene [41]. Thereby, limonene was decomposed into terpenes through isomerization reactions. A quantification study of the cracking products is recommended in future work.

Hence, the performance of toluene and limonene cracking over the various materials can be classified as follows: AC > BC_CG > BC_DS.

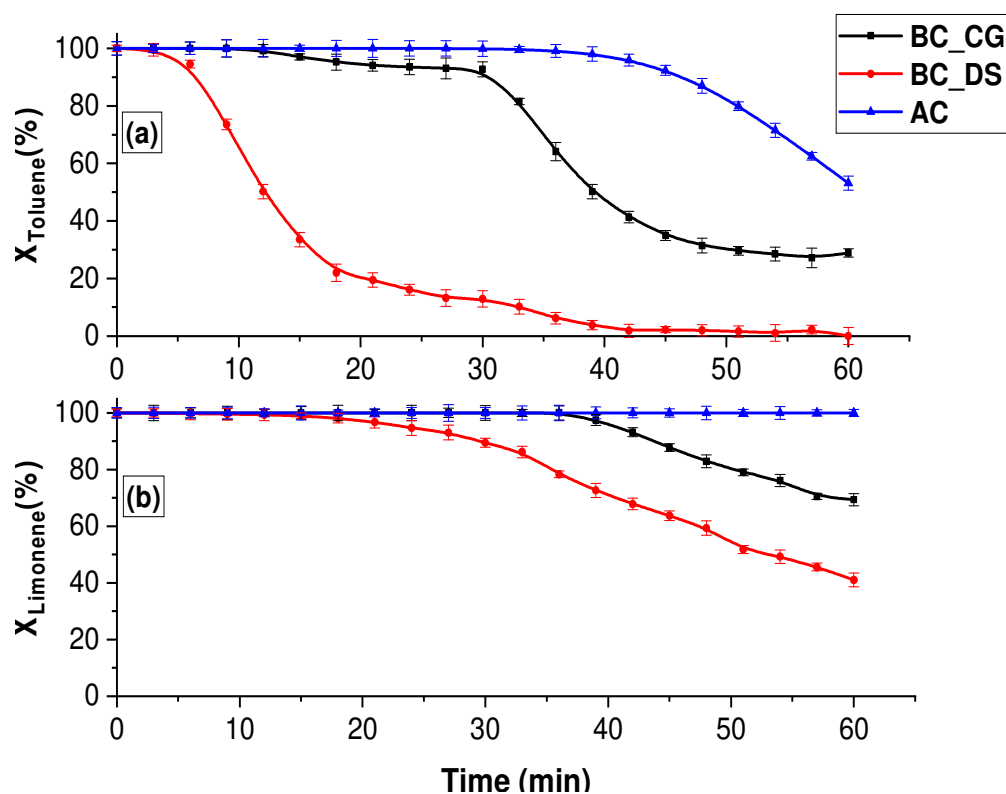


Fig. 5. Synthetic mixture 2, $t_{s2} = 2.50$ s; $T = 500$ °C : (a) Toluene conversion; (b) Limonene conversion.

The results of toluene and limonene cracking obtained in this work are compared with those in the literature (Table S2). It can be noted that the biochar from wood chips (pyrolyzed at 700 °C) used for toluene cracking tests leads to a cracking yield of 60.30 % at 900 °C [42]. In addition, the study of X. Liu et al. [43] on the catalytic reforming of toluene in the presence of activated carbon impregnated with nickel (10 % Ni/CA) at 500 °C indicates a toluene conversion rate of 24 %. These conversion rates are still much lower than that achieved by BC_CG. Hence, this biochar can be considered as an economical and promising material in the cracking of toluene present in the volatiles derived from the pyrolysis of used tires.

3.5 Analysis of the spent materials

The post-desulfurization characterization focuses on the two best performing materials used under the best operating conditions ($T= 500^{\circ}\text{C}$, $t_s= 2.50$ s, mixture 2): BC_CG and AC. The exhausted materials are named with the prefix "Spent". The characterization of these materials (with three repeated analyses) is summarized in Table S3. It is noted that Spent BC_CG and Spent AC show a mass loss of 2 % and 5 %, respectively. This mass loss can be explained by the reaction of limonene with the carbon surface of these materials. In addition, the H, N and S content also decreased slightly after use due to possible volatilization. This volatilization may also contribute to the observed mass losses. Furthermore, textural properties also play an important role in the catalytic activity of carbonaceous materials. Therefore, the porosity was studied by nitrogen adsorption at 77 K. It is noticed that the specific surface of Spent AC has improved. This slight increase reveals that the coke deposited during the cracking step has a porous character. It increased the specific surface area of the AC instead of blocking its original porous structure. This increase in specific surface area is followed by a decrease in mesopore volume, confirming that the mesopores are more involved in the adsorption/cracking mechanism. A similar observation is described by the recent work of Wang et al [44]. On the other hand, the specific surface area of BC_CG decreased against an increase in its micropore volume after use. This may result from the low activation of the biochar in the presence of CO_2 produced during the cracking tests.

4. Discussion : mechanisms of thiophene removal by biochar

Preliminary characterization of the biochar revealed that the thiophene adsorption process on its surface consists of a complex reaction mechanism involving the physicochemical properties of the biochar and the gas composition. In our case, it is still difficult to discriminate the individual contribution of each property to the thiophene removal capacity of BC_CG. However, the results showed that the critical biochar properties for good thiophene

removal are: mesoporous volume, acidic pH surface, presence of mineral species on the surface (especially P, K, Ca), nitrogen content, O-containing groups (especially acid groups), and the disorganized carbonaceous structure. The selectivity of adsorbents towards sulfur compounds depends on either physical (Vander Waals force) or chemical interaction (sigma and π bonds) between the adsorbate or target molecules (sulfur) and active sites on the adsorbent surface. Chemisorption follows mainly the combination or any one of the following mechanisms : π complexation, acid-base interaction, and direct sulfur-metal interaction. Physical adsorption via van der Waals forces does not control the selectivity of sulfur compounds [45]. The π -complexation interaction is stronger than the van der Waals interaction and aids higher selectivity to sulfur compounds than other compounds.

For AC, the large surface area overweighed other properties such as O-containing functional groups and aromaticity degree, making it different from biochar. Although the surface area (BET) of AC was almost sixteen times larger than BC_CG, its sorption capacity for thiophene was lower than that of BC_CG. This revealed that extremely high surface area and large pore volume of sorbent might not be the only criteria for efficient removal of thiophene. Previous work indicated that most thiophene sulfur compounds are Lewis base, which is easy to be adsorbed onto acid sites [46]. According to the X-ray spectroscopy (EDX, Fig. S 4) and CHNSO analysis results, the prominent proportions of P, K, and N can affect the acidic and basic properties of the carbon surface and thus influence the adsorption behavior [47]. Indeed, recently, Seredych and Bandosz. [48,49] reported that in addition of oxygen and other heteroatoms, such as sulfur and phosphorus in the activated carbon matrix, had a positive effect on its capacity and selectivity to separate DBT from model diesel fuel. This heteroatom (P) is usually bonded in the forms of phosphates. In this respect, it was revealed that phosphorus naturally contained in the carbon matrix of BC_CG can increase its acidity, enhancing the attraction of thiophene compounds, whose character is slightly basic.

Furthermore, in thiophene, S and C atoms have negative net charges, while H atoms have positive net charges [50]. In contrast, P and N atoms have positive and negative net charges, respectively. Thus, it is deduced that the S site with a negative net charge in thiophene tends to be adsorbed at P sites with positive net charges in π -conjugated carbon. A relevant study by Shimoyama and al. [51] dealing with the improvement of adsorptive desulfurization by P- and N-doped carbon materials, stated that phosphorus has a 10-20 times greater doping effect than nitrogen on thiophene adsorption. Therefore, these heteroatoms are important for improving the adsorptive desulfurization properties of carbon materials. To date, the mechanism of this effect is not well defined; we therefore suggest that the undoped BC_CG sample, naturally rich in N and P, may attract more of the thiophene molecule to its surface. In order to better study this effect, an X-ray photoelectron spectroscopy (XPS) analysis is recommended in future work. In addition, oxygen functional groups on the surface of the carbon material are also important for the removal of sulfur compounds in diesel fuel [52]. The sulfur atom has a pair of electrons on the six-electron π system, and another pair lies in the plane of the ring. The adsorbed amount of thiophene by BC_CG involves the transfer of electrons from the oxygen-containing functional groups due to π - π electron-donor interaction. The carboxylic acid groups on the surface of the biochar underwent as electron acceptors, forming a π - π electron acceptor-donor interaction with aromatic molecules, thus facilitating the adsorption of aromatic molecules. Different types of hydroxyl and amine groups in biochar can also be used as π electron donor sites. In this study, coke produced by the cracking of aromatic groups can itself form new functional groups that can then be cracked into CO, H₂, and CO₂ at high temperatures. Other active sites, such as the defects in graphene-like sheets, in addition to π interactions, can participate in the adsorption process of thiophene by BC_CG.

5. Regeneration

Regeneration of the best desulfurization candidate was performed according to the protocol described in Section 2.5. During CO₂ regeneration, multiple adsorption-desorption cycles were achieved (see Fig. S7 a). It's noted that the breakthrough time increased as the regeneration progressed and reached 28 min at the sixth adsorption with a maximum thiophene adsorption capacity of 1.84 mg/g. Beyond the sixth cycle, the breakthrough time (t_p) and the exhaustion time (t_e) decrease. The adsorbent is completely exhausted after 15 cycles of adsorption. On the other hand, thermal regeneration under nitrogen was also tested. No optimization of the operating conditions was performed due to resource constraints. Hence, the same CO₂ regeneration process was adopted, but using only pure nitrogen. The successive adsorption curves are shown in Fig. S7 b. It is clear that the breakthrough time doubled between the first adsorption and the second adsorption. However, after the first regeneration cycle, the breakthrough time gradually decreases and reaches about 1 min in the last thiophene adsorption cycle. The regeneration rate (RE) represents the adsorbed amount by the regenerated material n times the adsorbed amount of the same fresh material. It serves as an indicator of regeneration efficiency [53].

It is represented by the following expression :

$$RE (\%) = \frac{q_n}{q_{original}} \times 100 \quad (5)$$

Where q_n : the amount adsorbed by the regenerated adsorbent n times at a given equilibrium concentration (mg.g^{-1}); $q_{original}$: the quantity adsorbed by the fresh material at a given equilibrium concentration (mg.g^{-1}). The regeneration rate (RE) calculated for the two regeneration methods is presented in Fig. 6.

The improvement of BC_CG desulfurization capacities during the first six regeneration cycles under oxidizing atmosphere (CO₂/N₂), indicates that this method has positively affected the surface porosity of BC_CG. Indeed, the CO₂ burns the pore blocking structures created during

the catalytic cracking phase, developing a more porous structure. Hence, the elimination of these residues unblocks the pore entrances. This phenomena generates regeneration rates even higher than 100 % [54]. The performance of BC_CG reaches about 90 % after seven cycles. On the other hand, according to the regeneration rate (RE) the thiophene adsorption improved during the first cycle and then decreased significantly to 38 % in the 5th cycle. This can be explained by possible alterations in the surface chemistry of BC_CG, followed by a reduction of its surface area and deterioration of the pore structure. Thus, thermal regeneration led to a rapid decline in the adsorbent's performance. A similar result was found by Zeng et al. [55]. Although the high regeneration rate, successive cycles of heating and cooling can lead to mass loss and, very often, a significant deterioration of the adsorbent pore structure, thus reducing the final adsorption capacity and regeneration efficiency.

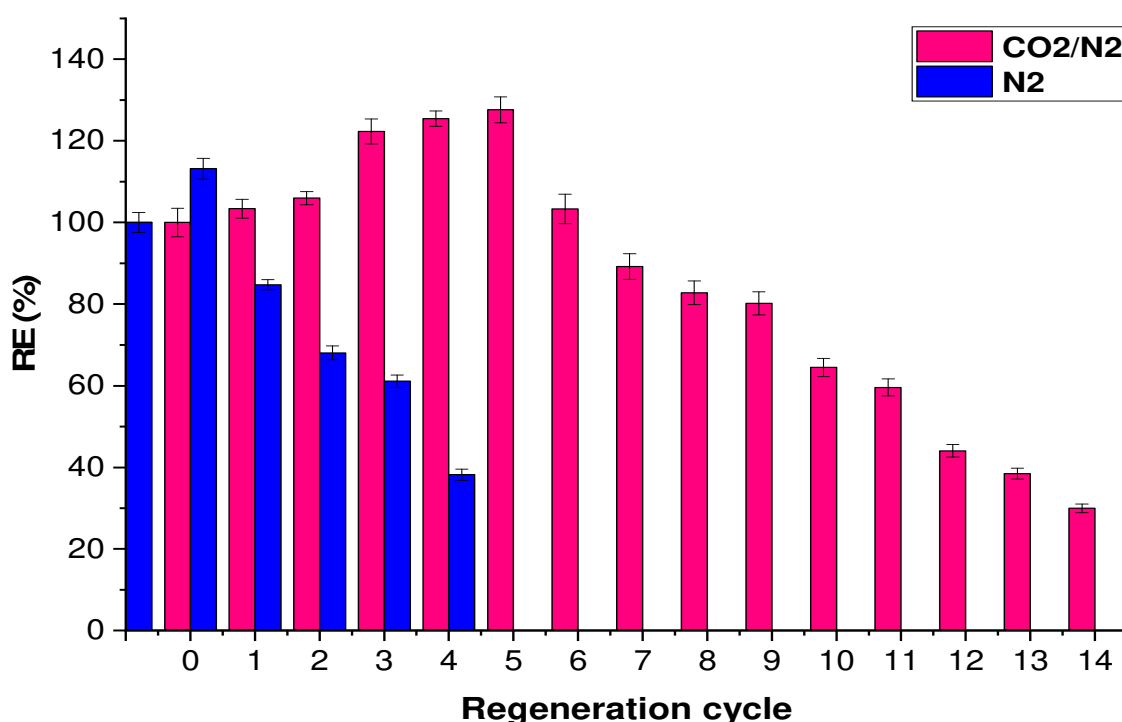


Fig. 6. Evolution of the regeneration rate according to the regeneration cycle/method.

According to the literature, thermal regeneration is the most widely used regeneration method and one of the most economical and efficient methods. On the other hand, several references have also applied regeneration by gasification using either steam or CO₂. The comparison of

the results of this study with the literature is presented in Table S4. The results of the present study show that the number of regeneration cycles achieved with CO₂ is relevant compared to other works. Thus, this research revealed that spent coffee grounds is an economic and accessible feedstock with great potential for biochar production, thiophene removal, good toluene cracking performance, and promising regeneration.

6. Characterization of the regenerated material

Biochars resulting from the last CO₂ and N₂ regeneration cycle were characterized. They are noted as follows: Spent BC_CG_CO₂ and Spent BC_CG_N₂, respectively. The elemental analysis, pH and mass loss of Spent BC_CG_CO₂ and Spent BC_CG_N₂ are listed in Table 4. CO₂ regeneration shows high O/C and (O+N)/C ratios, leading to low aromaticity and hydrophobicity compared to fresh BC_CG. In addition, an increase in the pH of Spent BC_CG_CO₂ and Spent BC_CG_N₂ is noted which confirms the adsorption process. Furthermore, a mass loss of about 14 % is reported under CO₂ regeneration against a decrease of 8 % during thermal regeneration. Indeed, in large-scale processes, the mass loss due to gasification must be added to other unavoidable losses, such as the loss occurring during loading and unloading of the adsorption beds. These handling losses can reach 15-20 % after six cycles [54].

The structural analysis shows a substantial decrease of approximately 96 % in the specific surface of Spent BC_CG_N₂ compared to that of fresh BC_CG with a reduction of the microporous volume. Therefore, it's assumed that the accumulation of coke on the biochar surface can lead to a loss of its activity [56]. On the other hand, a significant growth in the specific surface of Spent BC_CG_CO₂ is noted in comparison with fresh BC_CG. The specific surface area reaches a considerable value of 286.89 m²/g. In fact, in the presence of CO₂, the release of volatiles becomes more pronounced, leading to an increase in the specific surface area, the porosity, and the pores volume of the BC_CG. This improvement of the pore

structure facilitated the penetration of CO₂ into the channels and hence to be sufficiently in contact with the active sites and thus promote the gasification reaction. Thus, during the CO₂ regeneration, a cleavage of groups such as hydroxyl, methylene, methyl... etc., leads to a decrease in the mass of biochar [57]. Moreover, a more pronounced destruction of the mesoporosity is observed in the case of Spent BC_CG_N₂ than to that of Spent BC_CG_CO₂. This can lead us to understand the effectiveness of regeneration using an oxidizing agent versus simple thermal regeneration. When conventional techniques carry out regeneration, the decrease in the volume of the micropores is accompanied by a displacement towards pores of narrower sizes [58].

Table 4. Preliminary characterization of the regenerated carbonaceous material.

Materials	Spent BC_CG_CO₂	Spent BC_CG_N₂
Elemental and proximate analysis		
C	81.94±1.50	86.76±2.30
H	1.32±0.02	1.50±0.01
N	3.07±0.03	2.94±0.02
S	nd ¹	nd
O	6.67±0.24	1.80±0.01
H/C	0.016	0.017
O/C	0.081	0.021
(O+N)/C	0.119	0.055
pH	11.15±0.32	9.95±0.22
m (g)	48.12±0.50	51.56±0.35
Textural analysis		
S_{BET} (m²/g)	286.89±4.50	1.92±0.03
V_{micro} (cm³/g)	0.119±0.00	0.002±0.00
V_{meso} (cm³/g)	0.014±0.00	nd

¹ nd : not detected; traces: concentration below 0.06 wt %.

Fig. 7 illustrates the DFT analysis of BC_CG before and after N₂ and CO₂ regeneration. In the case of Spent BC_CG_N₂, the pore width became almost zero, indicating that the blocking of larger pores occurred to a large extent. This can be attributed to the deterioration of the pore structure due to the high regeneration temperature. On the other hand, a development of the microporosity of Spent BC_CG_CO₂ was observed. The micropore size of about 0.59 nm is similar to that of fresh AC. This micropore size is advantageous for thiophene adsorption whose critical diameter is 0.53 nm [59]. Hence, under a CO₂ atmosphere, the carbon

skeleton's partial gasification would better preserve the porous structure. In addition, the coke deposited on the biochar due to the catalytic decomposition could react with the CO₂ so that the texture blocking effect would be mitigated. Thus, the presence of CO₂ improves the textural properties of biochar and increases its lifespan.

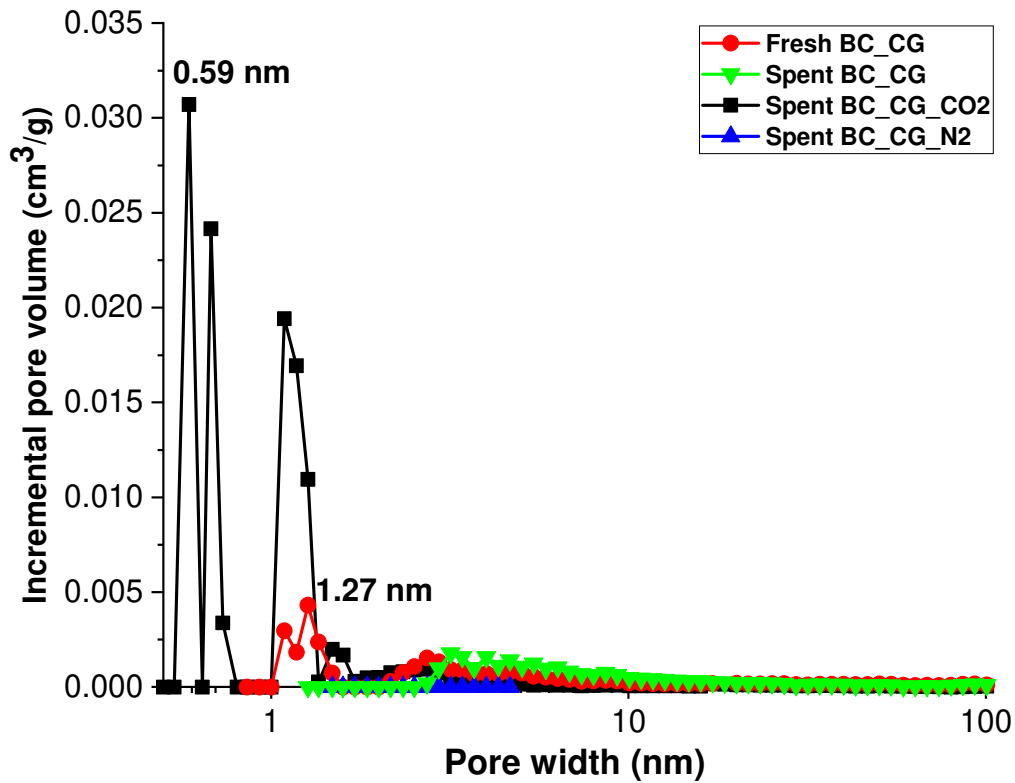


Fig. 7. Pore size distribution of Fresh BC_CG , Spent BC_CG , Spent BC_CG_CO₂, and Spent BC_CG_N₂.

The structures of Spent BC_CG , Spent BC_CG_CO₂, and Spent BC_CG_N₂ are presented in Fig. 8. We note that the biochar surface had become smoother, and the pores have widened due to the pores filling during the successive adsorption and desorption steps. Furthermore, following CO₂ regeneration, the surface seems to have a larger pore structure, and the micropores are easily visible (case of Spent BC_CG_CO₂). On the other hand, a porous destruction is observed by enlargement of the pores and a loss of structure between the adjacent pores at the end of the thermal regeneration (case of Spent BC_CG_N₂).

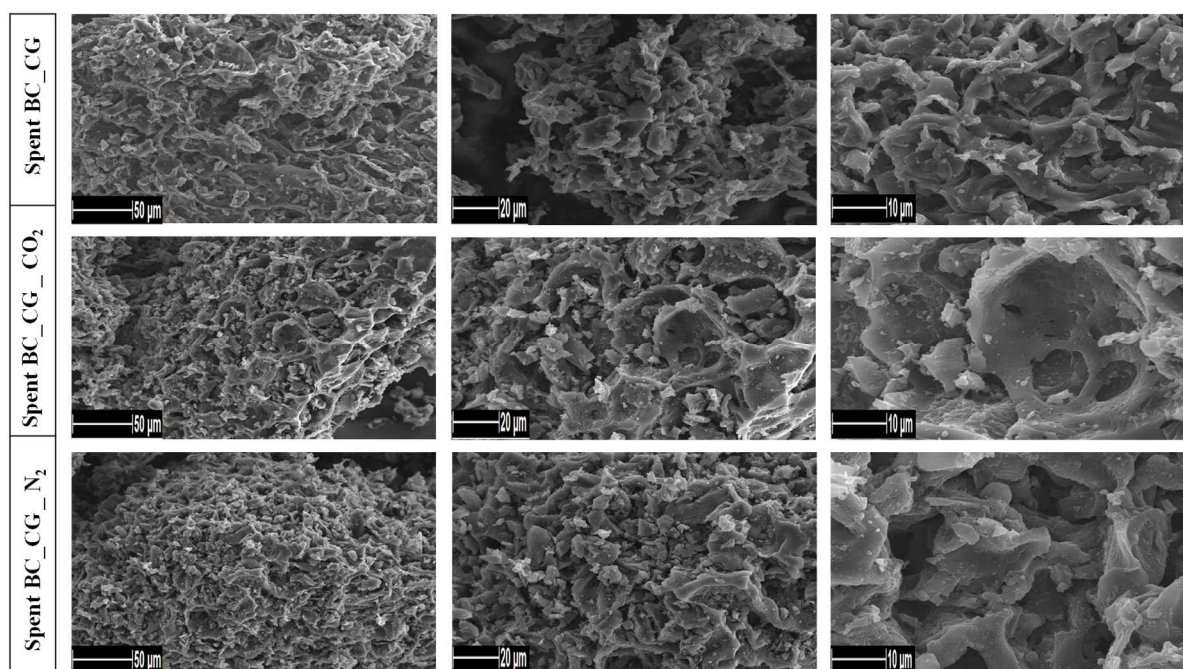


Fig. 8. SEM images of Spent BC_CG , Spent BC_CG_CO₂, and Spent BC_CG_N₂.

7. Conclusion

In the context of desulfurization of the volatiles derived from the waste tire pyrolysis (TDV), the present work aimed to identify a suitable biochar for the selective removal of thiophene and the tars cracking. For this purpose, two synthetic pyrolytic liquids were evaluated. Hence three materials were tested : biochar from spent coffee grounds (BC_CG), biochar from date seeds (BC_DS) and commercial activated carbon (AC). The effect of the operating conditions was also studied. The results showed that the spent coffee grounds biochar and commercial activated carbon present the best desulfurization results with adsorption values of 1.44 mg/g and 1.08 ± 0.02 mg/g respectively. In addition, BC_CG and AC showed the best catalytic activities for toluene cracking at 500 °C with an average conversion rate of 71 % and 91 % respectively. These carbonaceous materials contain K, Ca and Fe as well as functional groups that can act as active sites for adsorption in the ex-situ cracking. The valorization of biomass via pyrolysis has been proven to be a promising route to product a suitable biochar for thiophene adsorption TDV. From an economical and environmental point of view, it is

necessary to regenerate this adsorbent in order to be able to reuse it. Hence, two types of regeneration were tested : thermal regeneration and CO₂ regeneration. The BC_CG showed a promising regeneration capacities in the presence of CO₂ with 14 regeneration cycles.

Based on the above results, BC_CG exhibited better thiophene removal performance compared to the commercial activated carbon. Therefore, it can be concluded that BC_CG has a strong potential as an economical alternative adsorbent material for volatiles derived from used tires pyrolysis enhancement, which can also help decrease spent coffee grounds disposal problems.

Acknowledgements

This work has been partly carried-out in the frame of the partnership Hubert Curien Program through the PHC UTIQUE 2017 (Project code : 17G1139) and the authors gratefully acknowledge the support of the Mixt Franco-Tunisian Comity (CMCU). The authors are also grateful to the University of Gabes (Tunisia) for its supplementary financial support.

References

- [1] D. Czajczyńska, R. Krzyżyńska, H. Jouhara, N. Spencer, Use of pyrolytic gas from waste tire as a fuel: A review, *Energy*. 134 (2017) 1121–1131. <https://doi.org/10.1016/j.energy.2017.05.042>.
- [2] C. Sathiskumar, S. Karthikeyan, Recycling of waste tires and its energy storage application of by-products—a review, *Sustain. Mater. Technol.* 22 (2019) e00125.
- [3] K. Jadav, S. Pandian, A. Sircar, D. Subramanian, Investigation of nano catalyst to enhance fuel quality in waste tyre pyrolysis, *Energy Sources Part Recovery Util. Environ. Eff.* (2019) 1–10.
- [4] A.-M. Al-Lal, D. Bolonio, A. Llamas, M. Lapuerta, L. Canoira, Desulfurization of pyrolysis fuels obtained from waste: Lube oils, tires and plastics, *Fuel*. 150 (2015) 208–216. <https://doi.org/10.1016/j.fuel.2015.02.034>.
- [5] H. Aydın, C. İlkılıç, Optimization of fuel production from waste vehicle tires by pyrolysis and resembling to diesel fuel by various desulfurization methods, *Fuel*. 102 (2012) 605–612.
- [6] I. Hita, M. Arabiourrutia, M. Olazar, J. Bilbao, J.M. Arandes, P. Castaño, Opportunities and barriers for producing high quality fuels from the pyrolysis of scrap tires, *Renew. Sustain. Energy Rev.* 56 (2016) 745–759.
- [7] G.-G. Choi, S.-J. Oh, J.-S. Kim, Non-catalytic pyrolysis of scrap tires using a newly developed two-stage pyrolyzer for the production of a pyrolysis oil with a low sulfur content, *Appl. Energy*. 170 (2016) 140–147. <https://doi.org/10.1016/j.apenergy.2016.02.119>.
- [8] Y. Pan, D. Yang, K. Sun, X. Wang, Y. Zhou, Q. Huang, Pyrolytic transformation behavior of hydrocarbons and heteroatom compounds of scrap tire volatiles, *Fuel*. 276 (2020) 118095. <https://doi.org/10.1016/j.fuel.2020.118095>.

- [9] B. Saha, S. Vedachalam, A.K. Dalai, Review on recent advances in adsorptive desulfurization, *Fuel Process. Technol.* 214 (2021) 106685. <https://doi.org/10.1016/j.fuproc.2020.106685>.
- [10] W. Ahmad, Sulfur in petroleum: petroleum desulfurization techniques, in: *Appl. Nanotechnol. Desulfurization Process Pet. Eng.*, IGI Global, 2016: pp. 1–52.
- [11] A. Zhou, X. Ma, C. Song, Effects of oxidative modification of carbon surface on the adsorption of sulfur compounds in diesel fuel, *Appl. Catal. B Environ.* 87 (2009) 190–199.
- [12] P. Jeevanandam, K.J. Klabunde, S.H. Tetzler, Adsorption of thiophenes out of hydrocarbons using metal impregnated nanocrystalline aluminum oxide, *Microporous Mesoporous Mater.* 79 (2005) 101–110. <https://doi.org/10.1016/j.micromeso.2004.10.029>.
- [13] R. Wallace, S. Suresh, E.H. Fini, T.J. Bandosz, Efficient Air Desulfurization Catalysts Derived from Pig Manure Liquefaction Char, *C—Journal Carbon Res.* 3 (2017) 37. <https://doi.org/10.3390/c3040037>.
- [14] K.A. Motghare, A.P. Rathod, K.L. Wasewar, N.K. Labhsetwar, Comparative study of different waste biomass for energy application, *Waste Manag.* 47 (2016) 40–45.
- [15] GIFruits, Groupement Interprofessionnel des Fruits – Tunisie – www.gifruits.com. Accessed 2016 January, (2017). <http://gifruits.com/?p=3048&lang=fr> (accessed August 1, 2018).
- [16] S.I. Mussatto, L.M. Carneiro, J.P.A. Silva, I.C. Roberto, J.A. Teixeira, A study on chemical constituents and sugars extraction from spent coffee grounds, *Carbohydr. Polym.* 83 (2011) 368–374. <https://doi.org/10.1016/j.carbpol.2010.07.063>.

- [17] H. Aouled Mhemed, J. Largeau, S. Kordoghli, M. Marin Gallego, F. Zagrouba, M. Tazerout, Kinetic Study of Lignocellulosic Biomasses Pyrolysis Using Thermogravimetric Analysis, *Int. J. Biomass Renew.* 9 (2020) 25–41.
- [18] H. Aouled Mhemed, M. Marin Gallego, J.-F. Largeau, S. Kordoghli, F. Zagrouba, M. Tazerout, Gas adsorptive desulfurization of thiophene by spent coffee grounds-derived carbon optimized by response surface methodology: Isotherms and kinetics evaluation, *J. Environ. Chem. Eng.* (2020) 104036. <https://doi.org/10.1016/j.jece.2020.104036>.
- [19] B. Saha, S. Kumar, S. Sengupta, Green synthesis of nano silver on TiO₂ catalyst for application in oxidation of thiophene, *Chem. Eng. Sci.* 199 (2019) 332–341. <https://doi.org/10.1016/j.ces.2018.12.063>.
- [20] B. Saha, S. Sengupta, R. Selvin, Comparative studies of extraction ability of organic solvents to extract thiophene from model fuel, *Sep. Sci. Technol.* 55 (2020) 1123–1132. <https://doi.org/10.1080/01496395.2019.1580292>.
- [21] M. Królikowski, A. Lipińska, Separation of thiophene, or benzothiophene from model fuel using glycols. Liquid–liquid phase equilibria and oxidative desulfurization study, *Fluid Phase Equilibria.* 482 (2019) 11–23. <https://doi.org/10.1016/j.fluid.2018.10.017>.
- [22] W.L. McCabe, J.C. Smith, P. Harriott, Unit operations of chemical engineering, McGraw-hill New York, 1967.
- [23] F. Ji, C. Li, J. Xu, P. Liu, Dynamic adsorption of Cu(II) from aqueous solution by zeolite/cellulose acetate blend fiber in fixed-bed, *Colloids Surf. Physicochem. Eng. Asp.* 434 (2013) 88–94. <https://doi.org/10.1016/j.colsurfa.2013.05.045>.
- [24] S. Ma, H. Leong, L. He, Z. Xiong, H. Han, L. Jiang, Y. Wang, S. Hu, S. Su, J. Xiang, Effects of pressure and residence time on limonene production in waste tires pyrolysis process, *J. Anal. Appl. Pyrolysis.* (2020) 104899. <https://doi.org/10.1016/j.jaap.2020.104899>.

- [25] V. Benedetti, F. Patuzzi, M. Baratieri, Characterization of char from biomass gasification and its similarities with activated carbon in adsorption applications, *Appl. Energy*. 227 (2018) 92–99. <https://doi.org/10.1016/j.apenergy.2017.08.076>.
- [26] D. Kołodzyńska, J. Krukowska, P. Thomas, Comparison of sorption and desorption studies of heavy metal ions from biochar and commercial active carbon, *Chem. Eng. J.* 307 (2017) 353–363. <https://doi.org/10.1016/j.cej.2016.08.088>.
- [27] Q. Huang, P. Lu, B. Hu, Y. Chi, J. Yan, Cracking of Model Tar Species from the Gasification of Municipal Solid Waste Using Commercial and Waste-Derived Catalysts, *Energy Fuels*. 30 (2016) 5740–5748. <https://doi.org/10.1021/acs.energyfuels.6b00711>.
- [28] F.J. Sotomayor, K.A. Cychoz, M. Thommes, Characterization of micro/mesoporous materials by physisorption: concepts and case studies, *Acc Mater Surf Res*. 3 (2018) 36–37.
- [29] L. Qi, X. Tang, Z. Wang, X. Peng, Pore characterization of different types of coal from coal and gas outburst disaster sites using low temperature nitrogen adsorption approach, *Int. J. Min. Sci. Technol.* 27 (2017) 371–377. <https://doi.org/10.1016/j.ijmst.2017.01.005>.
- [30] X. Tang, Z. Wang, N. Ripepi, B. Kang, G. Yue, Adsorption Affinity of Different Types of Coal: Mean Isothermic Heat of Adsorption, *Energy Fuels*. 29 (2015) 3609–3615. <https://doi.org/10.1021/acs.energyfuels.5b00432>.
- [31] Z. Li, K. Wang, J. Song, Q. Xu, N. Kobayashi, Preparation of activated carbons from polycarbonate with chemical activation using response surface methodology, *J. Mater. Cycles Waste Manag.* 16 (2014) 359–366. <https://doi.org/10.1007/s10163-013-0196-8>.
- [32] T. Li, H. Tian, J. Chen, L. Cheng, Application of low pressure gas adsorption to the characterization of pore size distribution of shales: An example from Southeastern

- Chongqing area, China, *J. Nat. Gas Geosci.* 1 (2016) 221–230.
<https://doi.org/10.1016/j.jnggs.2016.07.001>.
- [33] W. Yang, S. He, G. Zhai, T. Dong, D. Gong, X. Yuan, S. Wei, Shale-gas accumulation and pore structure characteristics in the lower Cambrian Niutitang shales, Cen-gong Block, South China, *Aust. J. Earth Sci.* 66 (2019) 289–303.
<https://doi.org/10.1080/08120099.2018.1544172>.
- [34] R.W. Coughlin, F.S. Ezra, Role of surface acidity in the adsorption of organic pollutants on the surface of carbon, *Environ. Sci. Technol.* 2 (1968) 291–297.
- [35] A. Cabrera-Codony, E. Santos-Clotas, C.O. Ania, M.J. Martín, Competitive siloxane adsorption in multicomponent gas streams for biogas upgrading, *Chem. Eng. J.* 344 (2018) 565–573. <https://doi.org/10.1016/j.cej.2018.03.131>.
- [36] G. Shang, G. Shen, L. Liu, Q. Chen, Z. Xu, Kinetics and mechanisms of hydrogen sulfide adsorption by biochars, *Bioresour. Technol.* 133 (2013) 495–499.
<https://doi.org/10.1016/j.biortech.2013.01.114>.
- [37] N. Mohan, G.K. Kannan, S. Upendra, R. Subha, N.S. Kumar, Breakthrough of toluene vapours in granular activated carbon filled packed bed reactor, *J. Hazard. Mater.* 168 (2009) 777–781. <https://doi.org/10.1016/j.jhazmat.2009.02.079>.
- [38] Y. Yang, G. Lv, J. Li, W. Guo, Y. Zhang, Synthesis of ceria nanorods as adsorbent for the adsorption desulfurization of gasoline fuel, *J. Alloys Compd.* 747 (2018) 189–196.
<https://doi.org/10.1016/j.jallcom.2018.03.026>.
- [39] C. Delitala, E. Cadoni, D. Delpiano, D. Meloni, S. Melis, I. Ferino, Liquid-phase thiophene adsorption on MCM-22 zeolite and activated carbon, *Microporous Mesoporous Mater.* 110 (2008) 197–215.
<https://doi.org/10.1016/j.micromeso.2007.06.018>.

- [40] S.V. Patil, L.G. Sorokhaibam, V.M. Bhandari, D.J. Killedar, V.V. Ranade, Investigating role of sulphur specific carbon adsorbents in deep desulphurization, *J. Environ. Chem. Eng.* 2 (2014) 1495–1505. <https://doi.org/10.1016/j.jece.2014.07.009>.
- [41] C.P. Tavera Ruiz, P. Gauthier-Maradei, M. Capron, C. Pirez, O. Gardoll, B. Katryniok, F. Dumeignil, Transformation of dl Limonene into Aromatic Compounds Using Supported Heteropolyacid Catalysts, *Catal. Lett.* 149 (2019) 328–337. <https://doi.org/10.1007/s10562-018-2606-y>.
- [42] E. Cordioli, F. Patuzzi, M. Baratieri, Thermal and Catalytic Cracking of Toluene Using Char from Commercial Gasification Systems, *Energies.* 12 (2019) 3764. <https://doi.org/10.3390/en12193764>.
- [43] X. Liu, X. Yang, C. Liu, P. Chen, X. Yue, S. Zhang, Low-temperature catalytic steam reforming of toluene over activated carbon supported nickel catalysts, *J. Taiwan Inst. Chem. Eng.* 65 (2016) 233–241.
- [44] F. Wang, N. Gao, C. Quan, G. López, Investigation of hot char catalytic role in the pyrolysis of waste tires in a two-step process, *J. Anal. Appl. Pyrolysis.* 146 (2020) 104770. <https://doi.org/10.1016/j.jaap.2019.104770>.
- [45] X. Zhang, B. Gao, Y. Zheng, X. Hu, A.E. Creamer, M.D. Annable, Y. Li, Biochar for volatile organic compound (VOC) removal: Sorption performance and governing mechanisms, *Bioresour. Technol.* 245 (2017) 606–614. <https://doi.org/10.1016/j.biortech.2017.09.025>.
- [46] T.A. Saleh, G.I. Danmaliki, Influence of acidic and basic treatments of activated carbon derived from waste rubber tires on adsorptive desulfurization of thiophenes, *J. Taiwan Inst. Chem. Eng.* 60 (2016) 460–468. <https://doi.org/10.1016/j.jtice.2015.11.008>.
- [47] L.G. Sorokhaibam, V.M. Bhandari, M.S. Salvi, S. Jain, S.D. Hadawale, V.V. Ranade, Development of Newer Adsorbents: Activated Carbons Derived from Carbonized *Cassia*

fistula, Ind. Eng. Chem. Res. 54 (2015) 11844–11857.
<https://doi.org/10.1021/acs.iecr.5b02945>.

- [48] M. Seredych, T.J. Bandoz, Investigation of the enhancing effects of sulfur and/or oxygen functional groups of nanoporous carbons on adsorption of dibenzothiophenes, *Carbon*. 49 (2011) 1216–1224. <https://doi.org/10.1016/j.carbon.2010.11.038>.
- [49] M. Seredych, C.T. Wu, P. Brender, C.O. Ania, C. Vix-Guterl, T.J. Bandoz, Role of phosphorus in carbon matrix in desulfurization of diesel fuel using adsorption process, *Fuel*. 92 (2012) 318–326. <https://doi.org/10.1016/j.fuel.2011.08.007>.
- [50] J. Xiang, F. Zeng, H. Liang, B. Sun, L. Zhang, M. Li, J. Jia, Model construction of the macromolecular structure of Yanzhou Coal and its molecular simulation, *J. Fuel Chem. Technol.* 39 (2011) 481–488. [https://doi.org/10.1016/S1872-5813\(11\)60031-5](https://doi.org/10.1016/S1872-5813(11)60031-5).
- [51] I. Shimoyama, Y. Baba, Thiophene adsorption on phosphorus- and nitrogen-doped graphites: Control of desulfurization properties of carbon materials by heteroatom doping, *Carbon*. 98 (2016) 115–125. <https://doi.org/10.1016/j.carbon.2015.10.094>.
- [52] T.A. Saleh, K.O. Sulaiman, S.A. AL-Hammadi, H. Dafalla, G.I. Danmaliki, Adsorptive desulfurization of thiophene, benzothiophene and dibenzothiophene over activated carbon manganese oxide nanocomposite: with column system evaluation, *J. Clean. Prod.* 154 (2017) 401–412.
- [53] M. Miguet, Adsorption de COV issus d'eaux souterraines et régénération des charbons actifs par voie solaire, PhD Thesis, 2015.
- [54] F. Salvador, N. Martin-Sanchez, R. Sanchez-Hernandez, M.J. Sanchez-Montero, C. Izquierdo, Regeneration of carbonaceous adsorbents. Part I: Thermal Regeneration, *Microporous Mesoporous Mater.* 202 (2015) 259–276. <https://doi.org/10.1016/j.micromeso.2014.02.045>.

- [55] S. Zeng, Y.-K. Choi, E. Kan, Iron-activated bermudagrass-derived biochar for adsorption of aqueous sulfamethoxazole: Effects of iron impregnation ratio on biochar properties, adsorption, and regeneration, *Sci. Total Environ.* 750 (2021) 141691. <https://doi.org/10.1016/j.scitotenv.2020.141691>.
- [56] S. Hosokai, K. Kumabe, M. Ohshita, K. Norinaga, C.-Z. Li, J. Hayashi, Mechanism of decomposition of aromatics over charcoal and necessary condition for maintaining its activity, *Fuel*. 87 (2008) 2914–2922. <https://doi.org/10.1016/j.fuel.2008.04.019>.
- [57] S. Gao, J. Zhao, Z. Wang, J. Wang, Y. Fang, J. Huang, Effect of CO₂ on pyrolysis behaviors of lignite, *J. Fuel Chem. Technol.* 41 (2013) 257–264. [https://doi.org/10.1016/S1872-5813\(13\)60017-1](https://doi.org/10.1016/S1872-5813(13)60017-1).
- [58] C.O. Ania, J.B. Parra, J.A. Menéndez, J.J. Pis, Effect of microwave and conventional regeneration on the microporous and mesoporous network and on the adsorptive capacity of activated carbons, *Microporous Mesoporous Mater.* 85 (2005) 7–15. <https://doi.org/10.1016/j.micromeso.2005.06.013>.
- [59] C. Yu, X. Fan, L. Yu, T.J. Bandoz, Z. Zhao, J. Qiu, Adsorptive removal of thiophenic compounds from oils by activated carbon modified with concentrated nitric acid, *Energy Fuels*. 27 (2013) 1499–1505. <https://doi.org/10.1021/ef400029b>.